World Electric Vehicle Journal

MDPI

Article

Modeling and Experimental Investigation of Thermal Comfort and Energy Consumption in a Battery Electric Bus

Francesco Cigarini *, Tu-Anh Fay, Nikolay Artemenko and Dietmar Göhlich

Chair for Methods of Product Development and Mechatronics, Technische Unversität Berlin, Straße des 17. Juni 135, 10623 Berlin, Germany; tu-anh.fay@tu-berlin.de (T.-A.F.); n.artemenko@campus.tu-berlin.de (N.A.); dietmar.goehlich@tu-berlin.de (D.G.)

* Correspondence: f.cigarini@tu-berlin.de; Tel.: +49-(0)30-314-73895

Abstract: In battery electric buses (e-buses), the substantial energy consumption of the heating, ventilation, and air conditioning (HVAC) system can cause significant reductions of the available travel range. Additionally, HVAC systems are often operated at higher levels than what required for the thermal comfort of the passengers. Therefore, this paper proposes a method to experimentally investigate the influence of the HVAC system on the energy consumption and thermal comfort in a 12 m e-bus. An appropriate thermal comfort model is identified and the required climatic input parameters are selected and measured with self-developed sensor stations. The energy consumption of the e-bus, the state of charge (SoC) of the battery and the available travel range are measured by an embedded data logger. Climatic measurements are then performed with heating on and off on a Berlin bus line in winter conditions. The results show that the energy consumption of the e-bus is increased by a factor of 1.9 with heating on, while both the SoC and travel range are reduced accordingly. Comparing the thermal comfort with heating on and off, a decrease from "comfortable" to "slightly uncomfortable but acceptable" is observed.

Keywords: electric bus; energy consumption; HVAC system; modeling; thermal comfort

Citation: Cigarini, F.; Fay, T.-A.; Göhlich, D. Modeling and Experimental Investigation of Thermal Comfort and Energy Consumption in a Battery Electric Bus. *World Electr. Veh. J.* **2021**, *12*, 7. https://doi.org/10.3390/wevj12010007

Received: 27 November 2020
Accepted: 4 January 2021
Published: 6 January 2021

1. Introduction

In the year 2016 alone, the transport sector was responsible for about 16.2% of the total greenhouse gas (GHG) emissions worldwide [1]. This percentage is significantly higher in many industrialized countries, such as in the United States (29%) and in Germany (20%) [1]. According to the 2019 Global Carbon Budget [2], emissions from fossil fuels increased of 1.5% in 2017, 2.1% in 2018, and are projected to grow of 0.6% in 2019. It is estimated that approximately 75% of these emissions are originated from road transport [1] and especially in urban areas. In Germany, for example, approximately 40% of all CO_2 gases from road transport are emitted in cities [3]. Therefore, reducing emissions in urban areas is especially important to limit the overall release of GHGs from road transport on the global scale.

With the Climate Action Plan 2050, the German government has committed itself internationally and at European level to reduce its GHG emissions as stipulated by the 2016 Climate Paris Agreement [4]. By 2030, GHG emissions from the transport sector are to be reduced by 40% to 42% compared with the reference year 1990. Useful strategies to achieve this goal include promoting the use of battery electric vehicles (EVs) and strengthening the public transport system, which offers a lower-emissions alternative to private non-electric vehicles. Emissions can be even further reduced by the electrification of public transport and especially by replacing the currently employed gasoline and diesel buses with battery electric buses (e-buses).

According to the Berliner Mobilitätsgesetz (§26, 10) [5], the public transport system in Berlin is to be completely electrified by 2030. In this case, one of the main goals is the replacement of the diesel bus fleet with e-buses. However, this presents several significant challenges. For example, e-buses are typically characterized by a much shorter travel

range than diesel buses. Additionally, these properties are largely influenced by both the driving patterns and the use of auxiliary systems such as the heating, ventilation, and air conditioning (HVAC) system, which can cause decreases in travel range up to 50% when operated at maximum power [6].

The operation of the HVAC system in e-buses is based on norms and regulations (e.g., the VDV-Schrift 236 in Germany [7]), which, however, typically do not rely on empirical data to determine the thermal comfort of the passengers. This means that HVAC systems may be operated at higher levels than what is required for the comfort of the passengers, thereby leading to an unnecessary and significant reduction of the available travel range. New accurate guidelines based on empirical data are therefore necessary to optimize the operation of HVAC systems in e-buses. These data should include parameters such as the energy consumption of the HVAC sytem, the travel range of the bus and the thermal comfort of the passengers for several heating and cooling settings. Whereas information regarding the energy consumption of the HVAC system is typically available from the internal data loggers installed in most modern e-buses, thermal comfort models are typically required to assess the level of thermal well-being of the passengers [8]. Most of these models typically require knowledge about the bus internal climatic parameters [8], which can be measured via dedicated sensor systems. Additionally, information about the passengers (e.g., weight, height, thermal insulation of the clothing, etc.) is also necessary and can be gathered by means of personal surveys [8].

In this paper, a method for the experimental investigation of the thermal comfort of passengers and of the energy consumption of the HVAC system is developed and employed in a Solaris Urbino 12 e-bus (Solaris Bus & Coach, Owińska, Poland). To numerically determine the thermal comfort, a two-node model [8–10] is adopted. Based on the required model inputs, compact sensor stations are developed to measure the climatic parameters inside the e-bus. To reproduce realistic conditions, a group of test subjects is deployed on the e-bus in set of climatic measurements. These took place in winter during on-road operation on the 204 bus line of the Berlin public transport operator (Berliner Vekehrsbetriebe, BVG). Together with the climatic parameters, the energy consumed by the traction system and the HVAC system, the available travel range and the state of charge (SoC) of the battery are also measured by the embedded ViriCiti data logger (ViriCiti BV, Amsterdam, the Netherlands). Additionally, surveys are employed to gather the required personal information about the test subjects, as well as their perceived thermal comfort. To investigate the influence of the HVAC system's settings on the thermal comfort and energy consumption, the measurements are performed in both conditions of heating off and on. Finally, the acquired values are employed to compute the thermal comfort of the test subjects, which is then compared with the results of the surveys. The results of the computation and surveys are then evaluated together with the parameters measured by the data logger to investigate the influence of the HVAC system on the energy performance of the e-bus and the well-being of the test subjects.

This paper is organized as follows: in Section 2, the employed thermal comfort model is presented, whereas the design of the employed sensor stations is discussed in Section 3. The planning of the climatic measurements is shown in Section 4, whereas the measurements results are shown in Section 5 together with the thermal comfort parameters obtained from the computation and the surveys. The conclusions are presented in Section 6.

2. Thermal Comfort Model

Thermal comfort models are often employed to quantify the thermal sensation and well-being of human beings in response to environmental climatic conditions. Such models typically require measured climatic parameters (e.g., air temperature, air humidity, etc.) and information regarding the passengers as input for the computation [8].

Among the several thermal comfort models developed since the early 1970s, some of the most widely employed are the PMV-PPD [8,11] and the two-node model [8–10]. The first model enables to compute the comfort of a group of subjects by means of two parameters,

namely the predicted mean vote (PMV) and the predicted percentage of dissatisfied (PPD). Whereas the first parameter predicts the average thermal sensation based on the ASHRAE scale, the second estimates the percentage of test subjects who experience the environment as thermally unpleasant (corresponding to PMV < −1 or PMV > 1 [8]). The values of PMV and PPD are shown in Table 1. Notice that PMV = 0 corresponds to PPD = 5%. As the absolute value of PMV increases, the value of PPD increases exponentially.

Table 1. Values of predicted mean vote (PMV) and predicted percentage of dissatisfied (PPD).

PMV		PPD
Value (ASHRAE Scale)	**Average Thermal Sensation**	**Value (%)**
−3	cold	100%
−2	cool	99.8%
−1	slightly cool	45.4%
0	neutral	5%
1	slightly warm	45.4%
2	warm	99.8%
3	hot	100%

One of the main limitations of the PMV-PPD model is that it is only applicable to environments characterized by steady-state climatic conditions, such as those encountered in climatized buildings [8]. However, this is often not the situation for vehicles such as cars, buses or trains. In these cases, the thermal parameters can change significantly from one location to another inside the vehicle due to, e.g., the placement of the air outlet and the proximity to doors and windows. Additionally, the thermal conditions can also change significantly with time, due to, e.g., the opening and closing of doors. This is particularly relevant for buses used in public transportation because of the regular opening of the doors to let passengers in and out. This means that the climatic conditions in a bus are non-stationary and that the thermal comfort of the passengers can change greatly during their permanence onboard.

For environments characterized by non-stationary thermal conditions, the two-node model [8–10] is typically the preferred choice, as it enables to compute the thermal comfort throughout a given time interval and for transient thermal conditions. Similarly to the PMV-PPD model, it employs two parameters to quantify the thermal sensation (TSENS) and discomfort (DISC) of a group of people. These two parameters are time-dependent and are based on the extended ASHRAE scale shown in Table 2 [8].

Table 2. Values of thermal sensation (TSENS) and discomfort (DISC) according to the ASHRAE scale.

Value	TSENS	DISC
−5	intolerably cold	-
−4	very cold	-
−3	cold	-
−2	cool	-
−1	slightly cool	-
0	neutral	comfortable
1	slightly warm	slightly uncomfortable but acceptable
2	warm	uncomfortable and unpleasant
3	hot	very uncomfortable
4	very hot	limited tolerance
5	intolerably hot	intolerable

Because of the aforementioned properties, the two-node model is commonly used to investigate thermal comfort in cars [12,13] and buses [14]. Therefore, the two-node model is employed in this paper for the analyzed Solaris Urbino 12 e-bus.

Figure 1 shows a schematic representation of the employed thermal comfort model, which is discussed in detail together with its governing equations in Appendix A. As inputs, both information about the passengers and several climatic parameters are required. These are listed in Tables 3 and 4, respectively.

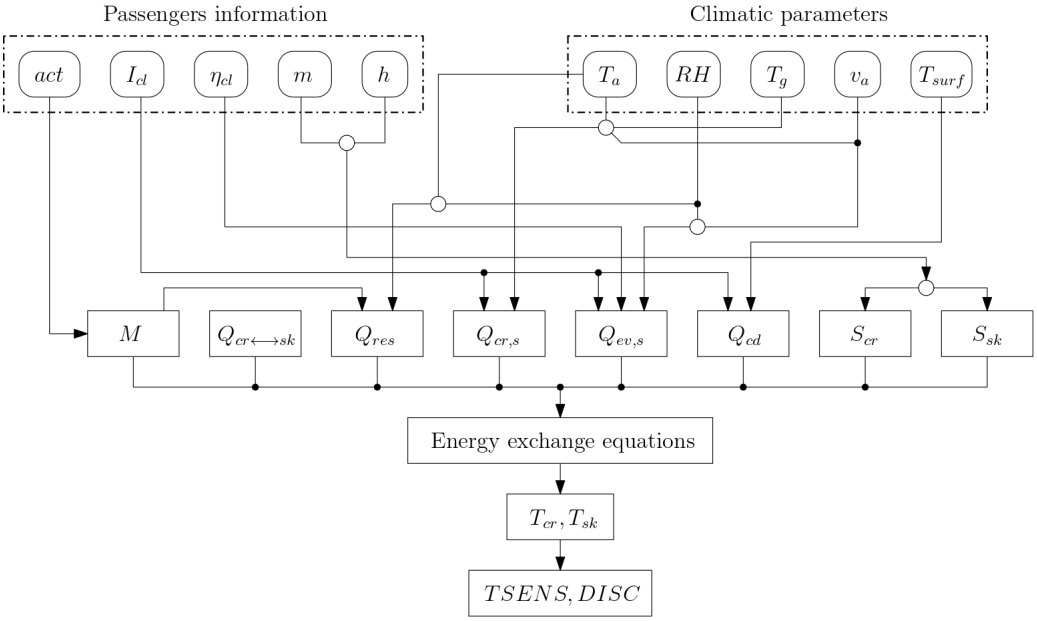

Figure 1. Schematic representation of the employed two-nodes thermal comfort model.

Table 3. Passenger parameters for the employed two-nodes thermal comfort model.

Parameter	Definition	Unit
η_{cl}	Clothes vapor permeation efficiency	-
act	Activity grade	act
h	Body height	m
$I_{clu,i}$	Thermal insulation of clothing	clo
m	Body mass	kg

Table 4. Climatic parameters for the employed two-nodes thermal comfort model.

Parameter	Definition	Unit
RH	Relative humidity of air	%
T_a	Air temperature	°C
T_g	Globe temperature	°C
T_{surf}	Temperature of the contacting surfaces	°C
v_a	Air velocity	m/s

3. Design of the Sensor Station

This section shows the design and development of the measurement electronics employed to monitor the climatic conditions inside a Solaris Urbino 12 e-bus. To assess the thermal comfort, all the parameters listed in Table 4 need to be measured. Additionally, measurement data points need to be stored at regular time intervals to properly characterize the variation of the climatic conditions with time. In this paper, the guidelines given by the GBK Standards (Gütegemeinschaft BusKomfort E.V.) are followed, and all climatic parameters are measured every 5 s.

Because of the limited space inside the e-bus, a compact sensor station concept is used in this paper, as schematically shown in Figure 2. The design is based on the already

available CoMoS comfort monitoring station [15] but includes four additional temperature sensors for the measurement of the contacting surface temperatures. Notice that all the sensors are connected to an ESP32 programmable microcontroller (Espressif Systems CO., LTD., Shanghai, China), which functions both as control unit and data logger. Six DS18B20+ Linear IC digital temperature sensors (Maxim Integrated Products, Inc., San Jose, CA, USA) are employed for the measurement of the air temperature and the contact surface temperature. Additionally, a temperature sensor is installed in a black sphere of diameter D_g = 40 mm for the measurement of the globe temperature. A Si7021 humidity sensor (Adafruit Industries, New York, NY, USA) and a Wind Sensor Rev. C. digital anemometer (Modern Device, Providence, RI, USA) are employed to measure the relative humidity and the air velocity, respectively. A DS3231 RTC digital clock (Adafruit Industries, New York, NY, USA) is employed to set the measurement time interval, whereas a SD card Reader (AZ Delivery, Deggendorf, Germany) is used to save the measured parameters locally on a SD card. Finally, a powerbank (Goobay, Latsia, Cyprus) is employed as power source for the electronics. The technical properties of the sensors are listed in Table 5.

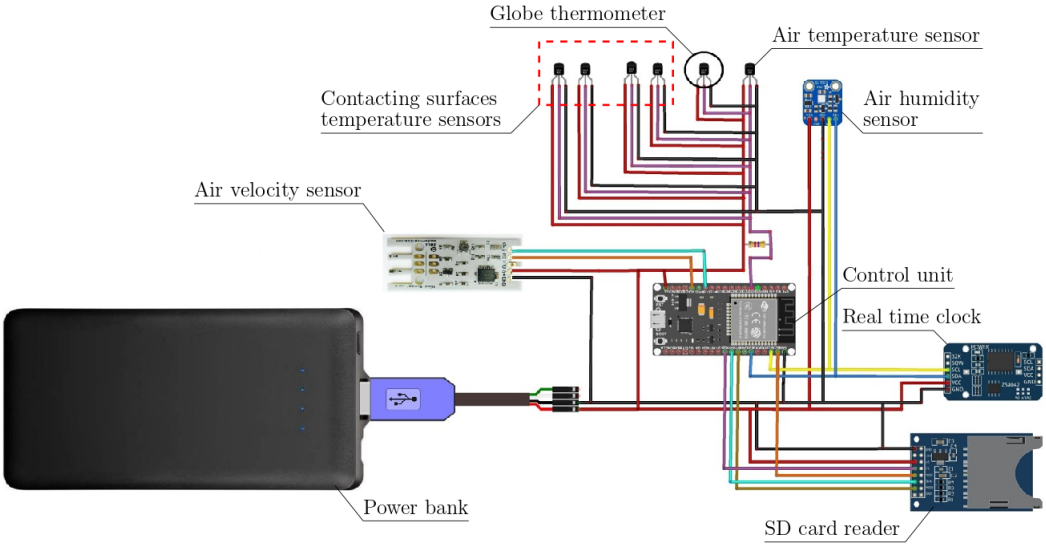

Figure 2. Schematic representation of the sensor station.

Table 5. Technical properties of the employed sensors.

Item	Definition	Measurement Range	Accuracy
DS18B20+ Linear IC digital	Temperature sensors	−55 °C–120 °C	±0.5 °C
Si7021	Humidity sensor	0–80%	3%
Wind Sensor Rev. C.	Air velocity sensor	0 m/s–26.8 m/s	-

The sensors need to be calibrated for high measuring accuracy. Therefore, the temperature sensors are submerged into an oil bath at constant temperature and the measured temperature is compared with the recorded temperature of a high-precision mercury thermometer for three temperature settings [16]. Additionally, the velocity sensors are calibrated by exposition to air currents with constant and homogeneous temperature inside an isolated room. The humidity sensors are already factory-calibrated.

4. Climatic Measurements: E-Bus, Bus Route, Sensor Stations Placement, and Measurement Plan

In this section, the e-bus employed for the measurements is shown. Additionally, the planning of the measurements and the disposition of the sensor stations inside the bus are presented.

4.1. Employed E-Bus

Figure 3 shows the Solaris Urbino 12 e-bus used for the measurements. The bus is approximately 12 m long and contains a single cabin for passengers. Additionally, it is equipped with two sliding doors for the entrance and exit of the passengers. A ViriCiti data logger is installed in the bus, thereby enabling the collection of data regarding the energy consumption of the traction and HVAC system, the SoC and the available travel range.

Figure 3. Solaris Urbino 12 e-bus (copyright Phototek | Fotographie & Film).

Figure 4 highlights the positioning of the sensor stations inside the e-bus. The climatic parameters are measured at three standing positions (crosses) and eight sitting positions (rhombi) and at breast height. Two sensor stations are positioned in close proximity to the doors to measure the air velocity due to the inflow of fresh air from the outer environment. The sensor stations at the sitting positions are equipped with additional sensors to measure the temperature of the seat contacting surfaces (as explained in Section 3).

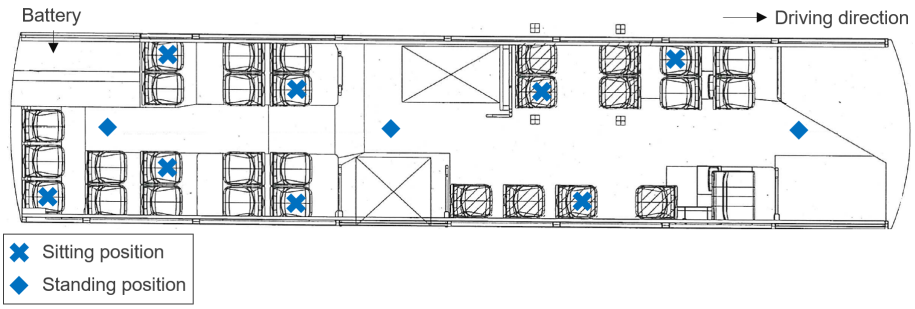

Figure 4. Positioning of the sensor stations in the bus.

In this paper, measurements are performed for both cases of heating off and on to evaluate the influence of the HVAC system's settings on the energy consumption of the e-bus and on the thermal comfort of the passengers. Due to the limited number of sensor stations, four measurements (two with heating on and two with heating off) were performed to assess the climatic parameters in the entire e-bus, as shown by the measurement plan in Table 6.

Table 6. Measurement plan.

Measurement	Duration (min)	Heating	Average External Temperature (°C)	Travelled Distance (km)	Number of Test Subjects
Meas. 1	35	off	4.3	8.1	11
Meas. 2	34		5.0	8.2	10
Meas. 3	38	on	7.8	8.1	12
Meas. 4	38		5.0	7.5	12

4.2. Bus Route

Figure 5a shows the BVG bus line 204 going from Hertzhallee to the train station S Südkreuz in Berlin. The measurements are designed to take place on the section of the line between Hertzallee and Münchener Straße because of the approximately constant topology, as shown by the altitude plot in Figure 5b. The Münchener Straße bus stop is chosen as turning point also because of a good turning option close to the line. The chosen bus route allows for a round trip duration between 34 min and 38 min.

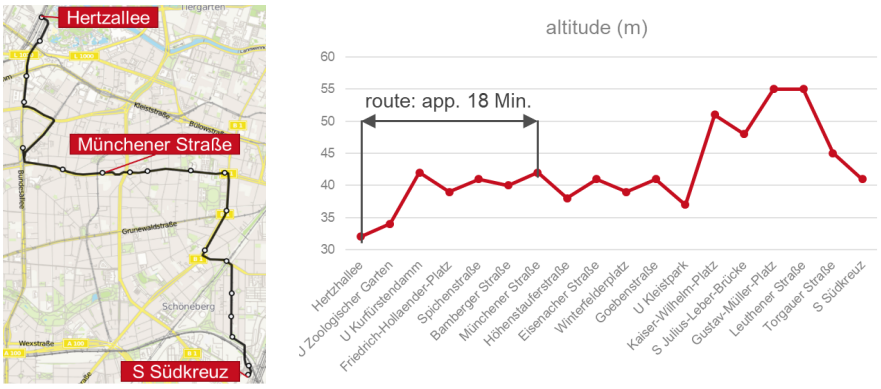

(**a**) Bus line 204 (**b**) Altitude of the bus stops on the bus line 204

Figure 5. Employed route for the measurements. The bus line 204 (**a**) and the altitude of the stops on the line (**b**) are shown.

5. Results

In this section, the results of the measurements are presented. The measurements took place on 21 February 2020 on the section of the BVG bus line 204 shown in Section 4.2. As a result, both the travelled distance and the travel duration were similar for all measurements. Additionally, a groups of test subjects was present on the bus during each measurement to gather the required personal information and to empirically investigate the perceived thermal sensation and comfort. For comparability of the results, groups of similar size were employed, as shown in Table 6.

As already discussed in Section 4.1, two measurements were performed with heating on and two with heating off to obtain a large set of data. However, the measured energy consumption and climatic parameters of the bus were very similar for measurements performed with the same heating settings. Therefore, in this paper only the measurement results of Meas. 1 and Meas. 3 are shown for simplicity of representation.

In Section 5.1, the measured energy consumption, SoC and travel range obtained from the ViriCiti data logger are shown, whereas in Section 5.2 the climatic parameters measured by the sensor stations are presented. Additionally, the results of the thermal comfort computation and of the surveys are discussed in Sections 5.3 and 5.4, respectively. Finally, Section 5.5 offers a short discussion of the results.

5.1. Data from the ViriCiti Data Logger

Figure 6 shows the energy consumption of the e-bus for both cases of heating off (blue, solid line) and on (red, dashed line). Notice that the energy consumption of the traction system (Figure 6a) is approximately the same for both measurements. The same is true for the auxiliary system (Figure 6c), which contains devices such as the motors for the bus doors and the head and rear lights. The operation of these sub-systems is independent from the settings of the HVAC system; therefore, their energy demand is approximately the same for both cases of heating off and on. The situation is very different for the energy used by the HVAC system (Figure 6b), which is approximately 0 kW h throughout Meas. 1 but increases progressively up to 7.4 kW h during Meas. 3. As a result, the total maximum energy consumption (Figure 6d) is increased by a factor of 1.9 from 9.2 kW h for Meas. 1 to 17.3 kW h for Meas. 3.

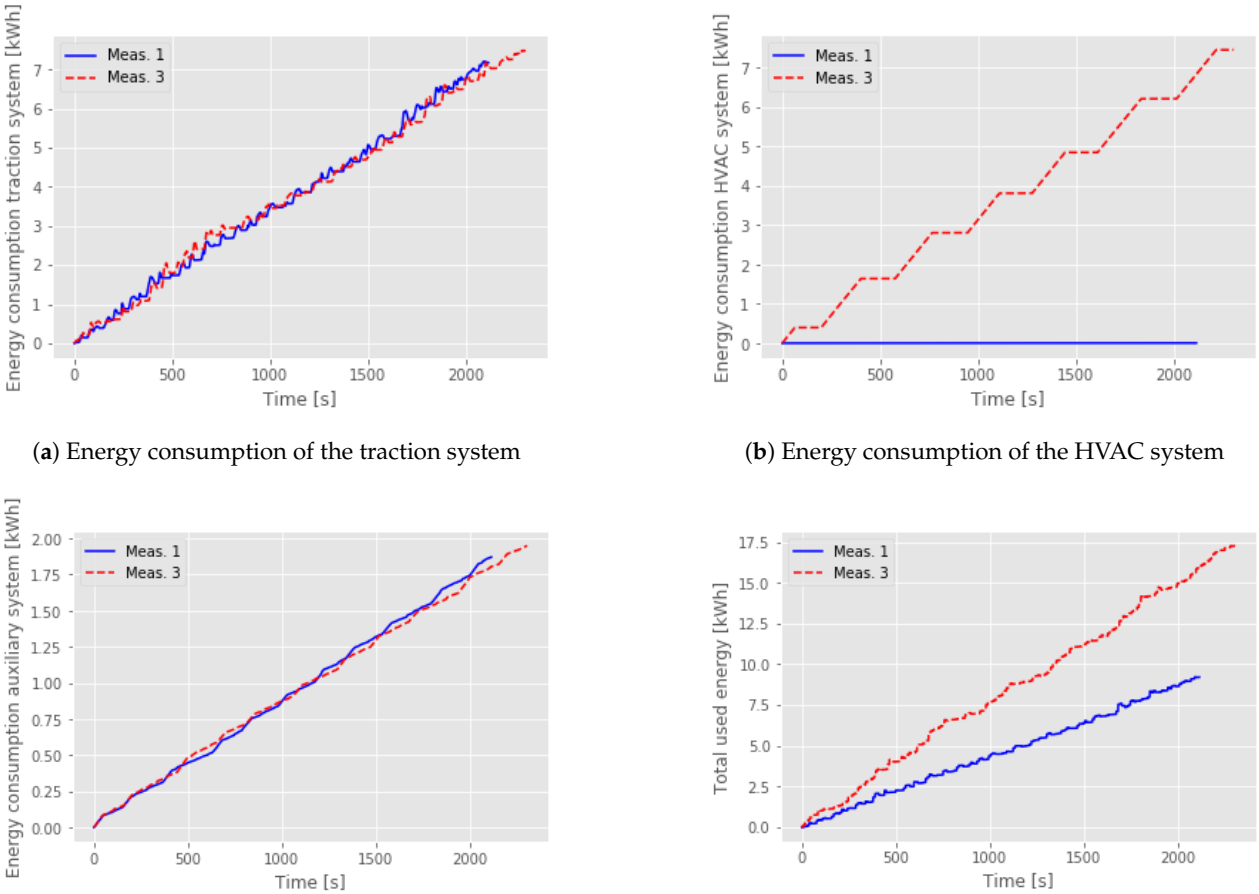

(**a**) Energy consumption of the traction system

(**b**) Energy consumption of the HVAC system

(**c**) Energy consumption of the auxiliary system

(**d**) Total used energy

Figure 6. Comparison of the energy consumption of the e-bus with heating off (Meas. 1, blue, solid line) and on (Meas. 3 red, dashed line). The energy consumption of (**a**) the traction system, (**b**) the heating, ventilation, and air conditioning (HVAC) system, and (**c**) the auxiliary system is shown, as well as (**d**) the total used energy.

The increased energy consumption results in an increased reduction of the SoC from −6% for Meas. 1 to −12% for Meas. 3, as shown in Figure 7a. In turn, this results in an increased reduction of the travel range from −6.8 km for Meas. 1 to −13.6 km for Meas. 3, as shown in Figure 7b. Notice that the energy consumption of the HVAC system, the SoC and the available travel range show stepwise variations. This is due to the acquisition algorithm of the ViriCiti data logger, which registers the change of these parameters in discrete steps. In Figures 6b and 7, the measured values are shown as lines for ease of representation.

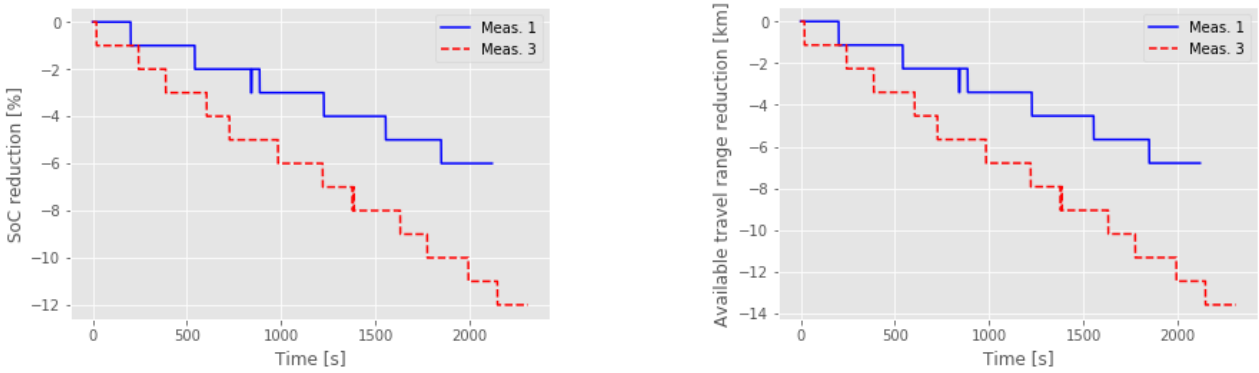

(**a**) Reduction of the State of Charge (SoC)

(**b**) Reduction of the available travel range

Figure 7. Comparison of the reduction of (**a**) the SoC and (**b**) of the available travel range in both cases of heating off (Meas. 1, blue, solid line) and on (Meas. 3, red, dashed line).

Table 7 lists the maximum energy comsumption, as well as the reduction of the SoC and of the travel range for both Meas. 1 and Meas. 3.

Table 7. Comparison of the maximum energy consumption, SoC and travel range reduction at the end of the Meas. 1 and Meas. 3.

Parameter	Meas. 1	Meas. 3
Total used energy (kW h)	9.2	17.3
Energy used by the traction system (kW h)	7.2	7.5
Energy used by the HVAC system (kW h)	0	7.4
Energy used by the auxiliary system (kW h)	1.9	1.9
SoC reduction (%)	−6.0	−12.0
Travel range reduction (km)	−6.8	−13.6

5.2. Measured Climatic Parameters

Figure 8 shows the average of the climatic parameters measured by all employed sensor stations for each measurement.

Table 8 lists the mean values and the standard deviations of each climatic parameter over the measurement time. Notice that the mean values of the air and globe temperatures increase of up to 7.0 °C when the heating is turned on. Concurrently, the mean air humidity decreases of up to 19.4%, indicating that the air becomes significantly drier when the heating is turned on. The mean air velocity is not affected signficantly by the HVAC system's settings (the high mean value of the air velocity in Meas. 3 is likely due to a hardware malfunction). The high values of the standard deviation in comparison with the mean value are due to the high peaks in the air velocity observed in Figure 8c. These peaks occur due to the inflow of air from the external environment at the opening and closing of the doors.

Table 8. Mean values and standard deviations of the measured climatic parameters over the measurement time.

Parameter	Meas. 1		Meas. 2		Meas. 3		Meas. 4	
	mean	std	mean	std	mean	std	mean	std
Air temperature (°C)	14.8	0.36	15.7	0.34	21.8	0.62	20.3	0.21
Relative air humidity (%)	49.5	0.96	47.5	0.97	30.1	1.45	32.8	0.21
Air velocity (m/s)	0.08	0.13	0.04	0.07	0.33	0.11	0.06	0.04
Globe temperature (°C)	13.8	0.4	14.8	0.37	21.1	0.58	19.3	0.18

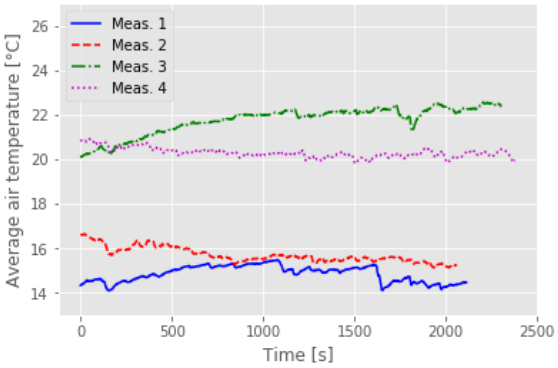

(**a**) Air temperature T_a

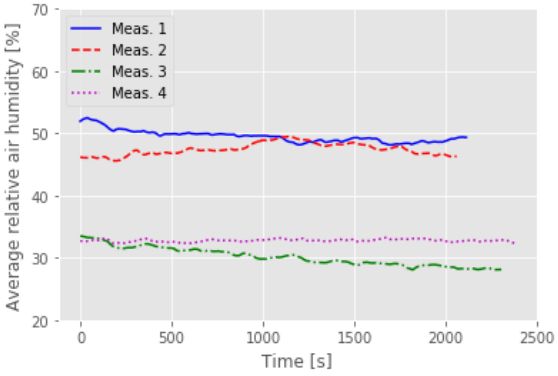

(**b**) Relative air humidity RH

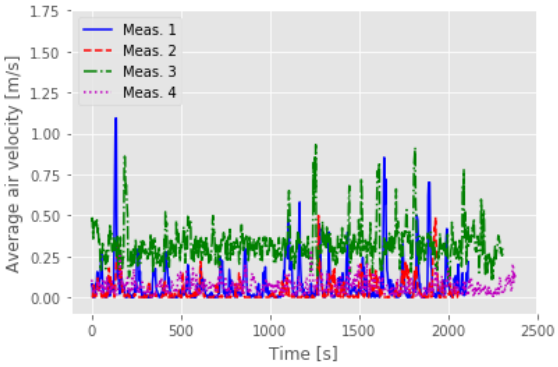

(**c**) Air velocity v_a

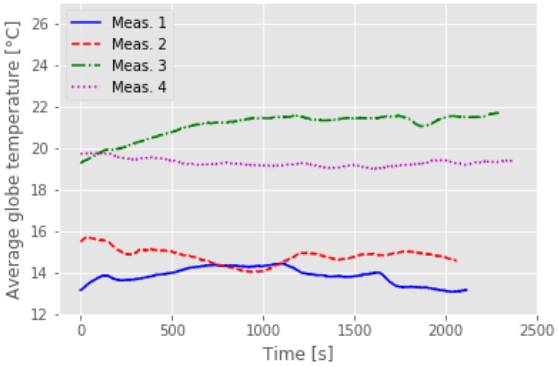

(**d**) Globe temperature T_g

Figure 8. Average measured climatic parameters for Meas. 1 (blue, solid line), Meas. 2 (red, dashed line), Meas. 3 (green, dash-dotted line) and Meas. 4 (purple, dotted line). (**a**) shows the air temperature, (**b**) the air humidity, (**c**) the air velocity, and (**d**) the globe temperature.

Figure 9 shows the average temperature of the seat contacting surface for all measurements. Notice that the seat temperature increases over time due to the warmth of the body.

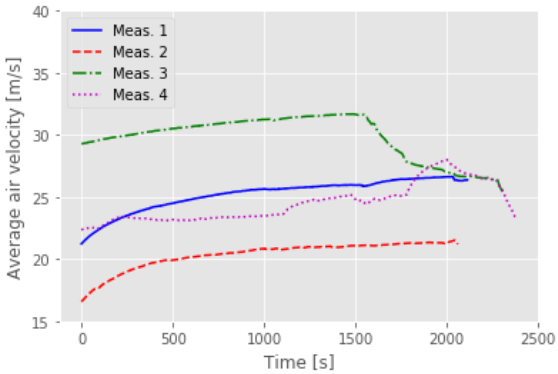

Figure 9. Temperature of the contacting surface of the seat for each measurement.

Notice from Figures 8 and 9 that all the measured climatic parameters change significantly with time. This justifies the use of the two-node thermal comfort model, as it is well-suited for non-stationary thermal conditions [8–10].

5.3. Computation of the Thermal Sensation and Thermal Comfort

Since the two-node model is only valid to estimate the average thermal comfort of a group of people [8–10], average climatic parameters for the two cases of standing and sitting passengers are employed to compute TSENS and DISC. Additionally, the needed personal information of the passengers (body mass, height, and overall thermal insulation of the clothing) are obtained by means of surveys and also averaged for the computation. The employed parameters of the test subjects are listed in Table 9.

Table 9. Parameters of the test subjects for the computation of the thermal comfort.

Parameter	Definition	Value
η_{cl}	Clothes vapor permeation efficiency	0.4
act	Activity grade	1.0 (sitting)/1.2 (standing)
h (m)	Body height	1.76
I_{cl} (clo)	Overall thermal insulation of the clothing	1.32
m (kg)	Body mass	74.1

These parameters are employed to compute the metabolic rates of heat production, the rates of heat exchange and heat loss and the temperatures of the skin and core compartments as discussed in Appendix A. These intermediate results are shown in Appendix B. Based on these values, the average thermal sensation TSENS and discomfort DISC are computed and shown in Figure 10 for Meas. 1 and Meas. 3 and both sitting and standing test subjects.

The end values of TSENS and DISC are listed in Table 10. For Meas. 1, these values are, respectively, −1.2 and 1.2 for sitting test subjects, corresponding approximately to "slightly cool" for TSENS and "slightly uncomfortable but acceptable" for DISC according to Table 2. For standing positions, the end values are both 0, corresponding to "neutral" for TSENS and "comfortable" for DISC. This difference is due to the higher rate of metabolic heat production M and lower rate of total heat loss Q_{tot} for standing than sitting test subjects, as shown in Appendix B.

For Meas. 3, the end values of TSENS and DISC are, respectively, −0.25 and 0.25 (for the sitting positions) and 0.25 and 0.2 (for the standing positions). These values correspond to approximately "neutral" for TSENS and "comfortable" for DISC. However, notice that TSENS is negative for sitting positions (denoting that TSENS is leaning towards "slightly cool") and positive for standing positions (denoting that TSENS is leaning towards "slightly warm"). As for Meas. 1, this is due to the higher value of M and lower value of Q_{tot} for standing than for sitting test subjects.

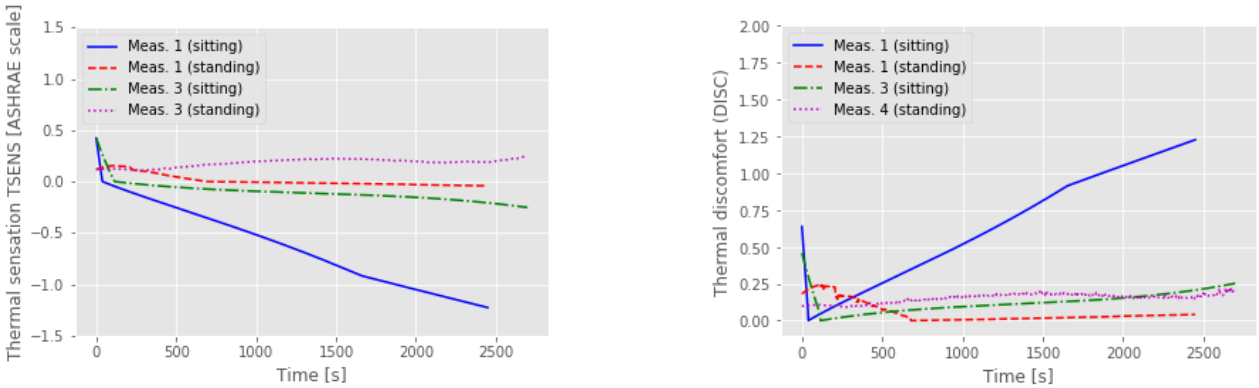

(**a**) Thermal sensation TSENS

(**b**) Thermal discomfort DISC

Figure 10. Computed (**a**) thermal sensation TSENS and (**b**) thermal discomfort DISC for Meas. 1 and Meas. 3 and for both sitting and standing test subjects.

Table 10. End values of TSENS and DISC for Meas. 1 and Meas. 3 and both sitting and standing test subjects.

Parameter	Meas. 1 (Sitting)	Meas. 1 (Standing)	Meas. 3 (Sitting)	Meas. 3 (Standing)
TSENS	−1.2	0.0	−0.25	0.25
DISC	1.2	0.0	0.25	0.2

5.4. Results of the Passengers Survey

To empirically evaluate the results of the computation, the thermal sensation and comfort of the test subjects are surveyed by means of direct questionnaires. The results are shown in Figures 11 and 12 for both Meas. 1 and Meas. 3.

Notice the change in thermal sensation when the heating is turned on:

- the total percentage of test subject perceiving the environment as cool or cold decreases from 90.9% to 41.7%,
- the total percentage of test subject perceiving the environment as neutral increases from 9.1% to 16.7%, and
- the total percentage of test subject perceiving the environment as warm or hot increases from 0.0% to 41.6%.

Concurrently, the thermal comfort is also affected when the heating is turned on:

- the total percentage of test subject perceiving the environment as comfortable increases from 27.3% to 41.7%,
- the total percentage of test subject perceiving the environment as slightly uncomfortable increases from 45.5% to 50.0%, and
- the total percentage of test subject perceiving the environment as uncomfortable or very uncomfortable decreases from 27.3% to 8.3%.

The average thermal sensation and thermal comfort obtained from the surveys are listed in Table 11 for Meas. 1 and Meas. 3 and both sitting and standing test subjects.

Notice that for the case of sitting subjects the values obtained from the survey are very close to the values computed from the model and shown in Table 10 for both measurements. However, a larger deviation can be observed for standing positions and especially for Meas. 1. This is most likely due to the limited number of test subjects in standing positions, which may affects the statistic reliability of the survey's results.

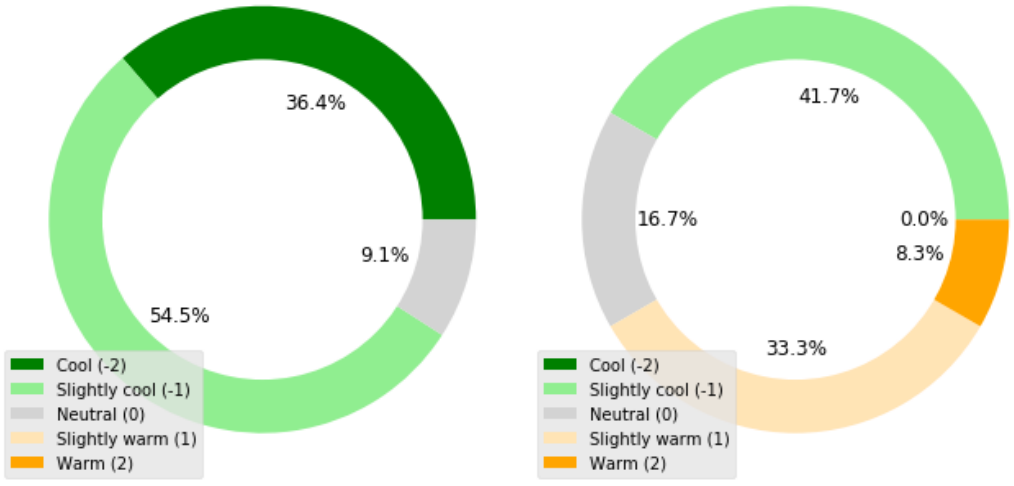

(**a**) Thermal sensation-Meas. 1 (**b**) Thermal sensation-Meas. 3

Figure 11. Results of the passengers survey. (**a**,**b**) show the thermal sensation of all the test subjects for Meas. 1 and Meas. 3, respectively.

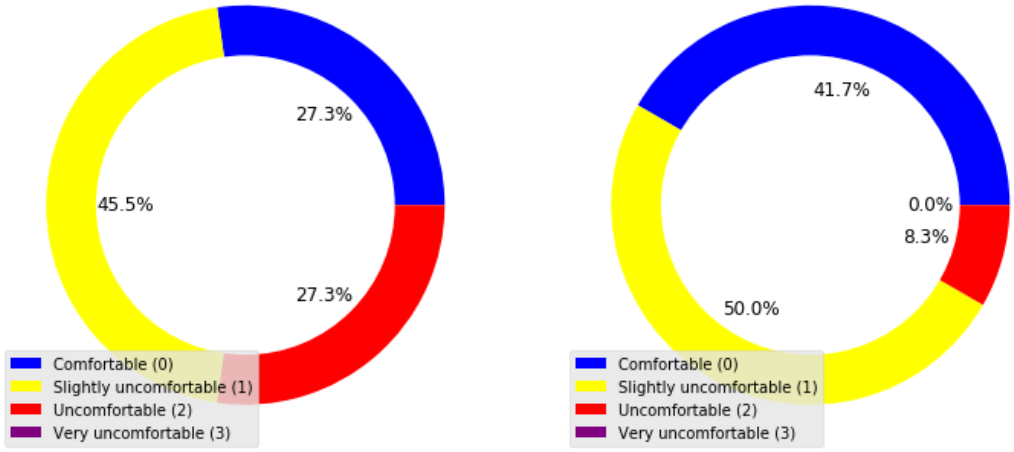

(**a**) Thermal comfort-Meas. 1 (**b**) Thermal comfort-Meas. 3

Figure 12. Results of the passengers survey. (**a**,**b**) show the thermal comfort of all the test subjects for Meas. 1 and Meas. 3, respectively.

Table 11. Average thermal sensation and comfort of the test subjects obtained from the survey.

Parameter	Meas. 1 (Sitting)	Meas. 1 (Standing)	Meas. 3 (Sitting)	Meas. 3 (Standing)
Thermal sensation	−1.25	−1.3	−0.1	0.7
Thermal comfort	1.0	1.0	0.6	1.0

5.5. Discussion of the Results

The results of the computation in Section 5.3 confirm that the HVAC system has an influence on both the thermal sensation and comfort of the test subjects, as TSENS increases from a minimum of −1.2 with heating off up to a maximum of 0.25 with heating on, whereas DISC decreases from a maximum of 1.2 with heating off down to a minimum of 0.2 with heating on. However, this transition is not very large, as the corresponding perception of the climatic conditions only changes from "slightly cool" and "slightly uncomfortable but tolerable" with heating off to "neutral" and "comfortable" with heating on. The benefit of the HVAC system is even less clear when considering the results of surveys shown in Section 5.4. In this case, the average thermal comfort only improves for sitting subjects from 1.0 with heating off to 0.6 with heating on, whereas it remains unchanged for standing test subjects. Conversely, the results presented in Section 5.1 clearly show that the HVAC system has a strong impact on the operation of the e-bus, as it results in an increase of the total used energy by a factor of 1.9. Consequently, this causes an increase of the SoC reduction and of the travel range reduction by a factor of 2.0.

Overall, the presented results clearly show that the developed method is highly efficient to investigate the influence of the HVAC system on the energy efficiency and thermal comfort in e-buses. Additionally, both the computation and survey results strongly indicate that the limitations to the operation of e-buses due to the HVAC system may largely outweigh the benefits on the thermal comfort of the passengers. Finally, they also suggest that the currently employed norms (such as the German *VDV-Schrift 236* [7]) may lead to operation of the HVAC system at levels higher than what is needed for the thermal well-being of the passengers.

6. Conclusions and Next Steps

In this paper, a method is presented to experimentally investigate the energy consumption of the HVAC system and the thermal comfort of the passengers in a Solaris Urbino 12 e-bus. This method employs the embedded ViriCiti data logger to monitor parameters such as the used energy, the state of charge (SoC) of the battery and the available travel range of the e-bus. Additionally, the climatic conditions inside the bus are measured via self-developed sensor stations and employed together with the personal information of the test subjects as inputs of a a two-node model. As a result, the thermal sensation TSENS and discomfort DISC are computed. To test this method, four climatic measurements are performed in an e-bus in Berlin with winter conditions. To investigate the relation between the set inner room temperature, the energy consumption and the thermal comfort, these measurements are performed for both cases of heating off and on. The experimental results show that the HVAC system causes a large increase of the total used energy of a factor 1.9, together with an increased reduction of the SoC and travel range of a factor 2.0. However, the benefit of the HVAC system on the thermal comfort of the passengers is relatively low, as the value of DISC only decreases from a maximum end value of 1.2 for heating off (corresponding approximately to a perceived "slightly uncomfortable but tolerable" environment) to a minimum end value of 0.2 for heating on (corresponding approximately to a perceived "comfortable" environment). These findings are corroborated by the results of the surveys, which show that the average thermal comfort of the test subjects only changes from a maximum value of 1.0 with heating off to a minimum value of 0.6 with heating on. These results indicate that the current regulation for the operation of the HVAC systems in e-buses may need to be revised to enable passenger comfort, while improving the energy efficiency (and, consequently, the travel range). Additionally, they show that the developed method is well-suited to quantitatively analyze both the energy consumption and the thermal comfort in e-buses.

In the next steps, the employed thermal comfort model will be validated by comparing the computed TSENS and DISC with the empirical thermal sensation and comfort obtained by surveying a larger sample of passengers via questionnaires. Additionally, the developed method will be also employed for summer operation to investigate the effect of the air conditioning settings on both the energy consumption and the thermal comfort.

Author Contributions: Conceptualization, F.C. and T.-A.F.; model development, F.C.; electronics development, F.C. and N.A.; climatic measurements, F.C. and N.A.; data analysis an simulation, F.C. and N.A.; writing–original draft preparation, F.C. and T.-A.F.; writing–review, D.G.; writing–review and editing, F.C. and T.-A.F.; supervision, F.C.; project administration, T.-A.F.; funding acquisition, D.G. All authors have read and agreed to the published version of the manuscript.

Funding: The authors gratefully acknowledge the financial support of the German federal government. Parts of this work have been supported by the Federal Ministry of Transportation and Digital Infrastructure (Project "E-MetroBus", grant number 3EMF0105B).

Acknowledgments: The authors wish to thank the partners from the Berlin public transport operator (Berliner Verkehrsbetriebe, BVG) for the inspiring discussions and their valuable support. Furthermore, the authors wish to acknowledge Vivekanandan Gopalakrishnan Divyaa and Ganesh Purushothaman from SASTRA Deemed University for the support in the research, as well as Hansjörg Rotheudt and Michael Schaub from the Hermann-Rietschel Institute (TU Berlin) for the support in the development and calibration of the sensor stations.

Conflicts of Interest: The authors declare no conflict of interest.

Appendix A. Governing Equations of the Employed Thermal Comfort Model

The two-node model considers the human body as thermally divided in two separate compartments, namely the core (represented as a grey disk in Figure A1) and the skin compartment (yellow disk in Figure A1). The body is separated from the external environment by the clothing (black circle in Figure A1).

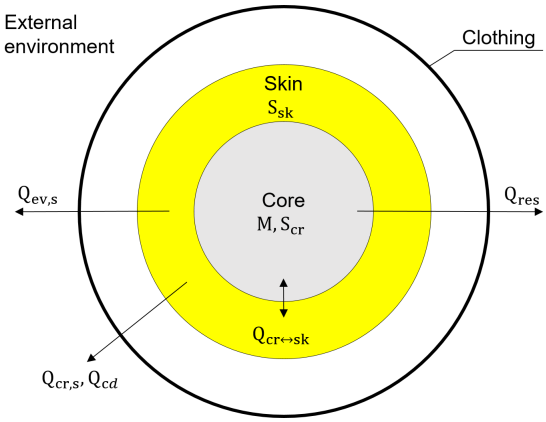

Figure A1. Graphic representation of the two-node model. The core and skin compartment are depicted as a grey and yellow disk, respectively, whereas the clothing is represented as a black circle.

The energy exchange between the core compartment, the skin compartment and the external environment is governed by the energy balance equations:

$$M = Q_{res} + Q_{cr\longleftrightarrow sk} + S_{cr}, \tag{A1}$$

for the core compartment and:

$$Q_{cr\longleftrightarrow sk} = Q_{cr,s} + Q_{ev,s} + Q_{cd} + S_{sk}, \tag{A2}$$

for the skin compartment [8–10]. In Equations (A1) and (A2) M is the net metabolic rate of heat production of the human body, S_{cr} and S_{sk} the rates of heat storage in the core and skin compartments, respectively, $Q_{cr\longleftrightarrow sk}$ the rate of heat exchanged between the core and skin compartments, Q_{res} the total rate of heat loss by respiration, $Q_{cr,s}$ and $Q_{ev,s}$, respectively, the rates of sensible heat loss by convection and radiation and of evaporative heat loss and Q_{cd} the rate of heat loss by conduction. These parameters are determined from the personal information about the test subjects and the climatic parameters of thee-bus as discussed in the following sections.

Appendix A.1. Net Metabolic Rate of Heat Production

The net metabolic rate of heat production represents the heat generated by the human body. This can be determined as [8]:

$$M = M_{met} + M_{shiv} - W, \tag{A3}$$

where M_{met}, M_{shiv} and W are, respectively, the basal rate of metabolic heat production, the rate of metabolic heat generated by shivering and the rate of mechanical work produced. The value of M_{met} is computed as [17]:

$$M_{met} = 58.15 \cdot act, \tag{A4}$$

where act is the activity grade of the body and is typically determined from look-up tables [8]. The value of M_{shiv} can be determined as [14]:

$$M_{shiv} = 19.4 \cdot CSIG_{sk} \cdot CSIG_{cr}, \tag{A5}$$

where $CSIG_{sk}$ and $CSIG_{cr}$ are, respectively, the cold signal of the skin and the core compartments, defined as [14]:

$$\begin{aligned} CSIG_{cr} &= T_{cr,set} - T_{cr} \quad if \quad T_{cr} < T_{cr,set}, \\ CSIG_{cr} &= 0\,°\text{C} \qquad\quad if \quad T_{cr} \geq T_{cr,set}, \end{aligned} \tag{A6}$$

and:

$$\begin{aligned} CSIG_{sk} &= T_{sk,set} - T_{sk} \quad if \quad T_{sk} < T_{sk,set}, \\ CSIG_{sk} &= 0\,°C \qquad\quad if \quad T_{sk} \geq T_{sk,set}. \end{aligned} \tag{A7}$$

In Equations (A6) and (A7), T_{cr} and T_{sk} are, respectively, the core and skin temperatures, whereas $T_{cr,set}$ =37.0 °C and $T_{sk,set}$ =34.0 °C are respecitvely the setpoint core and skin temperatures [8,14].

The rate of mechanical work W is approximately zero in both cases of sitting or standing passengers in a bus and can therefore be neglected in Equation (A3) [14].

Appendix A.2. Rates of Heat Storage

The rate of heat storage in the body is equal to the rate of increase or decrease in internal energy [8] and is expressed as:

$$S_{cr} = c_{p,b} \cdot \frac{m \cdot (1-\alpha)}{A_b} \cdot \frac{dT_{cr}}{dt}, \tag{A8}$$

for the core and:

$$S_{sk} = c_{p,b} \cdot \frac{m \cdot \alpha}{A_b} \cdot \frac{dT_{sk}}{dt}, \tag{A9}$$

for the skin compartment [8]. In Equations (A8) and (A9) $c_{p,b} = 3500\,\mathrm{J/(kg \cdot K)}$ is the specific heat of the human body, m is the body mass, α is the fraction of the total body mass thermally contained in the skin compartment, A_b the body surface area and t the time. The value of α is computed as [8]:

$$\alpha = 0.0418 + \frac{0.745}{3600 \cdot q_{bl} + 0.585}, \tag{A10}$$

where the peripheral blood flow q_{bl} is computed as [14]:

$$q_{bl} = \frac{6.3 + 50 \cdot WSIG_{cr}}{3600 \cdot (1 + 0.5 \cdot CSIG_{sk})}. \tag{A11}$$

In Equation (A11), $WSIG_{cr}$ is the warm signal from the core, determined as [14]:

$$\begin{aligned} WSIG_{cr} &= 0\,°C \quad if \quad T_{cr} \leq T_{cr,set}, \\ WSIG_{cr} &= T_{cr} - T_{cr,set} \quad if \quad T_{cr} > T_{cr,set}. \end{aligned} \tag{A12}$$

The value of A_b is computed from the body mass m and height h as [18]:

$$A_b = 0.202 \cdot m^{0.425} \cdot h^{0.725}, \tag{A13}$$

Appendix A.3. Rate of Heat Exchanged between the Core and Skin Compartments

The rate of heat exchange between core and skin compartments $Q_{cr \longleftrightarrow sk}$ is computed as [8]:

$$Q_{cr \longleftrightarrow sk} = k_{cr \longleftrightarrow sk} \cdot \rho_{bl} \cdot c_{p,bl} \cdot q_{bl} \cdot (T_{cr} - T_{sk}), \tag{A14}$$

where $k_{cr \longleftrightarrow sk}$ =5.28 $\mathrm{W/(m^2K)}$ is the effective heat transfer coefficient between core and skin, whereas $c_{p,bl}$ =4190 $\mathrm{J/(kg \cdot K)}$ and ρ_{bl} =1.06 kg/L are, respectively, the specific heat and the mass density of blood.

Appendix A.4. Total Rate of Heat Loss by Respiration

The total rate of heat loss by respiration Q_{res} can be computed as [8]:

$$Q_{res} = 0.0014 \cdot M \cdot (34 - T_a) + 0.0173 \cdot M \cdot (5.87 - p_a), \tag{A15}$$

where T_a is the air temperature and p_a is the water vapor pressure in ambient air. This can be determined from the relative air humidity RH as [14]:

$$p_a = 6.1 \cdot RH \cdot exp\left(\frac{17.269 \cdot T_{sk}}{T_{sk} + 237.3}\right), \tag{A16}$$

Appendix A.5. Total Rate of Sensible Heat Loss by Convection and Radiation

The total rate of heat loss by convection and radiation $Q_{cr,s}$ can be computed as [8]:

$$Q_{cr,s} = \frac{T_{sk} - T_0}{R_{cl} + 1/(f_{cl} \cdot (h_r + h_c))}, \tag{A17}$$

where T_0 is the operative temperature, R_{cl} and f_{cl} are, respectively, the thermal resistance of the clothes and the clothing area factor, whereas h_c and h_r are, respectively, the convective and radiative heat transfer coefficients. The value of T_0 is determined from the mean radiant temperature MRT as [8]:

$$T_0 = \frac{h_r \cdot MRT + h_c \cdot T_a}{h_r + h_c}. \tag{A18}$$

The value of MRT is typically determined from the measured air velocity v_a and the globe temperature T_g as [19]:

$$MRT = \left[(T_g + 273)^4 + 1.1 \times 10^8 \frac{v_a^{0.6}}{\epsilon \cdot D^{0.4} \cdot (T_g - T_a)}\right]^{1/4} - 273, \tag{A19}$$

where D and ϵ are, respectively, the diameter and emissivity of the globe thermometer employed to measure T_g. For a black globe, ϵ = 0.95. The value of R_{cl} is determined as [8]:

$$R_{cl} = 0.155 \cdot I_{cl}, \tag{A20}$$

where I_{cl} is the overall thermal insulation of clothing. This is determined from the thermal insulation $I_{clu,i}$ of each garment as [8]:

$$I_{cl} = \sum_i I_{clu,i} + 0.161, \tag{A21}$$

where $I_{clu,i}$ is obtained from look-up tables for each garment [8]. The value of f_{cl} can also be estimated from I_{cl} as [8]:

$$\begin{aligned} f_{cl} &= 1 + 0.2 \cdot I_{cl} \quad if \quad I_{cl} \leq 0.5\,\text{clo}, \\ f_{cl} &= 1.05 + 0.1 \cdot I_{cl} \quad if \quad I_{cl} > 0.5\,\text{clo}. \end{aligned} \tag{A22}$$

The value of h_r is constant and equal to 4.7 $\text{W}/(\text{m}^2\text{K})$ for typical indoor temperatures. Instead, the value of h_c is dependant of the air velocity v_a. For sitting subjects, h_c is computed as [8,20]:

$$\begin{aligned} h_c &= 3.1\,\text{W}/(\text{m}^2\text{K}) \quad if \quad v_a \leq 0.2\,\text{m/s}, \\ h_c &= 8.3 \cdot v_a^{0.6} \quad if \quad 0.2\,\text{m/s} < v_a \leq 4\,\text{m/s}, \end{aligned} \tag{A23}$$

whereas for standing subjects, it is determined as [8,21]:

$$\begin{aligned} h_c &= 4\,\text{W}/(\text{m}^2\text{K}) \quad if \quad v_a \leq 0.15\,\text{m/s}, \\ h_c &= 14.8 \cdot v_a^{0.69} \quad if \quad 0.15\,\text{m/s} < v_a \leq 1.5\,\text{m/s}, \end{aligned} \tag{A24}$$

Appendix A.6. Total Rate of Evaporative Heat Loss

The total rate of evaporative heat loss $Q_{ev,s}$ is computed as [8]:

$$Q_{ev,s} = w\frac{p_{sk,s} - pa}{R_{e,cl} + 1/(f_{cl} \cdot h_e)} = w \cdot E_{max}, \tag{A25}$$

where w is the skin wettedness, $R_{e,cl}$ the evaporative thermal resistance of the clothes, h_e the evaporative heat transfer coefficient and E_{max} the maximum possible evaporative heat loss. The value of w is determined as [8]:

$$w = 0.06 + 0.94 \cdot \frac{E_{rsw}}{E_{max}}, \tag{A26}$$

where E_{rsw} is the rate of regulatory sweat generation. This is defined as [8]:

$$E_{rsw} = 4.7 \times 10^{-5} \cdot h_{fg} \cdot WSIG_b \cdot exp(WSIG_{sk}/10.7). \tag{A27}$$

In Equation (A27) $WSIG_b$ is the warm signal from the body, defined as [8]:

$$\begin{aligned} WSIG_b &= 0\,°C \quad if \quad T_b \leq T_{b,set}, \\ WSIG_b &= T_b - T_{b,set} \quad if \quad T_{cr} > T_{b,set}, \end{aligned} \tag{A28}$$

where T_b and $T_{b,set}$ = 36.49 °C are, respectively, the temperature and the setpoint temperatures of the body. The value of T_b is computed from T_{sk} and T_{cr} as: [8]

$$T_b = (1 - \alpha) \cdot T_{cr} + \alpha \cdot T_{sk}. \tag{A29}$$

The evaporative thermal resistance of the clothes $R_{e,cl}$ is computed as [8]:

$$R_{e,cl} = \frac{R_{cl}}{\eta_{cl} \cdot LR}, \tag{A30}$$

where η_{cl} and LR are, respectively, the clothes vapor permeation efficiency and the Lewis ratio. The value of η_{cl} varies between 0.34 and 0.41 for most clothing ensembles and can be determined from look-up tables [8]. The value of the Lewis ratio LR is determined as [8]:

$$LR = 15.15 \cdot \frac{T_{sk} + 273.2}{273.2}. \tag{A31}$$

The value of h_e is determined as [8]:

$$h_e = h_c \cdot LR. \tag{A32}$$

Appendix A.7. Total Rate of Heat Loss by Conduction

The total rate of heat loss by conduction represents the heat transmitted at the interface between the body and any contacting objects. The value of Q_{cd} is determined as [17]

$$Q_{cd} = \frac{T_{sk} - T_{surf}}{R_{cl}}, \tag{A33}$$

where T_{surf} is the temperature of the contacting surfaces. In the case of a bus, such surfaces are the seats on which the passengers sit.

Appendix A.8. Thermal Comfort Parameters

Combining Equations (A1), (A2), (A8) and (A9) yields:

$$c_{p,b} \cdot \frac{m \cdot (1 - \alpha)}{A_b} \cdot \frac{dT_{cr}}{dt} = M - (Q_{res} + Q_{cr \longleftrightarrow sk}). \tag{A34}$$

for the core compartment and:

$$c_{p,b} \cdot \frac{m \cdot \alpha}{A_b} \cdot \frac{dT_{sk}}{dt} = Q_{cr \longleftrightarrow sk} - (Q_{cr_sk} + Q_{ev_sk} + Q_{cd}). \tag{A35}$$

for the skin compartment. Equations (A34) and (A35) can be solved to yield the values of T_{cr} and T_{sk} as a function of the time t. As a result, the temperature of the body can be computed according to Equation (A29). and employed to compute the two parameter TSENS and DISC [8]:

$$\begin{aligned} TSENS &= 0.4685 \cdot (T_b - T_{b,c}) \quad if \quad T_b < T_{b,c}, \\ TSENS &= 4.7 \cdot \eta_{ev} \cdot \frac{T_b - T_{b,c}}{T_{b,h} - T_{b,c}} \quad if \quad T_{b,c} \leq T_b \leq T_{b,h}, \\ TSENS &= 4.7 \cdot \eta_{ev} + 0.4685 \cdot (T_b - T_{b,h}) \quad if \quad T_b > T_{b,h}, \end{aligned} \tag{A36}$$

and:

$$\begin{aligned} DISC &= 0.4685 \cdot (T_b - T_{b,c}) \quad if \quad T_b < T_{b,c}, \\ DISC &= \frac{4.7 \cdot (E_{rsw} - E_{rsw,req})}{E_{max} - E_{rsw,req} - E_{dif}} \quad if \quad T_b \geq T_{b,c}, \end{aligned} \tag{A37}$$

where η_{ev} = 0.85 is the evaporative efficiency, $E_{rsw,req}$ the required value of E_{rsw} providing thermal comfort, E_{dif} the evaporation by diffusion, whereas $T_{b,c}$ and $T_{b,h}$ are the lower and upper limits for the zone of evaporative regulation. The values of $E_{rsw,req}$ and E_{dif} are determined as:

$$E_{rsw,req} = 0.42 \cdot (M - 58.15), \tag{A38}$$

and:

$$E_{dif} = 0.06 \cdot (1 - w_{rsw}) \cdot E_{max}, \tag{A39}$$

where w_{rsw} is the portion of the body that must be wetted to evaporate the regulatory sweat and is determined as:

$$w_{rsw} = \frac{E_{rsw}}{E_{max}}. \tag{A40}$$

Finally, $T_{b,c}$ and $T_{b,h}$ are defined as:

$$T_{b,c} = \frac{0.194}{58.15} \cdot (M - W) + 36.301, \tag{A41}$$

and:

$$T_{b,h} = \frac{0.347}{58.15} \cdot (M - W) + 36.669. \tag{A42}$$

The mathematical constants for the computation of TSENS and DISC are listed in Table A1.

Table A1. Constants for the computation of TSENS and DISC.

Constant	Definition	Value	Unit
ϵ	Emissivity of black globe	0.95	-
η_{ev}	Evaporative efficiency	0.85	-
ρ_{bl}	Blood mass density	1.06	kg/L
$c_{p,a}$	Specific heat of air	1005	J/(kg · K)
$c_{p,b}$	Specific heat of the human body	3500	J/(kg · K)
$c_{p,bl}$	Specific heat of blood	4190	J/(kg · K)
h_{fg}	Heat of vaporization of water	2.43×10^6	J/kg
h_r	Radiative heat transfer coefficient	4.7	W/(m^{2}K)
$k_{cr \longleftrightarrow sk}$	Effective heat transfer coefficient between core and skin	5.28	W/(m^{2}K)
p_t	Barometric pressure	101.325	kPa
$T_{b,set}$	Temperature setpoint of the body	36.49	°C
$T_{cr,set}$	Temperature setpoint of the core	37	°C
$T_{sk,set}$	Temperature setpoint of the skin	34	°C

Appendix B. Intermediate Computation Results

The parameters listed in Table 9 are employed together with the measured climatic parameters (see Section 5.2) to compute the metabolic rates of heat production, as well as the rates heat exchange and heat loss according to Equations (A3), (A14), (A15), (A17) and (A25). These are shown in Figure A2 for Meas. 1 and Meas. 3 and for both cases of sitting and standing positions. Additionally, the rate of total heat loss $Q_{tot} = Q_{res} + Q_{cr,s} + Q_{ev,s} + Q_{cd}$ is also shown for each measurement.

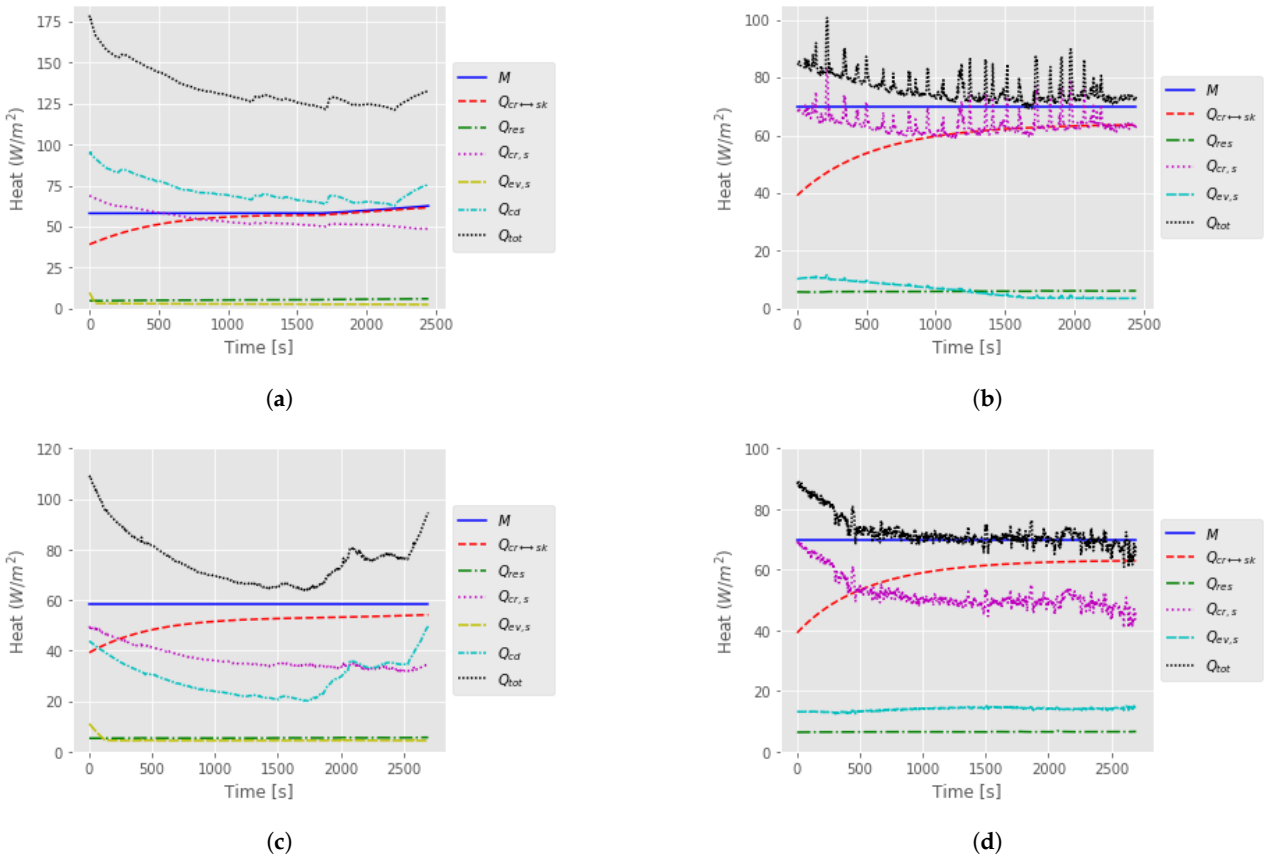

Figure A2. Computed average metabolic rates of heat production, rates of heat exchange and rates of heat loss for Meas. 1 and 3 and both sitting and standing positions. (**a**) Meas. 1 (sitting positions). (**b**) Meas. 1 (standing positions). (**c**) Meas. 3 (sitting positions). (**d**) Meas. 3 (standing positions).

Notice that for all measurements the largest heat losses are due to convection and radiation through the skin ($Q_{cr,s}$) and to conduction (Q_{cd}). This results in a higher average rate of total heat loss for the sitting than for the standing positions due to the absence of conduction heat losses for the standing case (see Table A2), as already noted in Section 5.3. This is particularly apparent for Meas. 1, where the average rate of total heat loss is 134.2 $W/(m^2K)$ for sitting positions and 76.4 $W/(m^2K)$ for standing positions.

Table A2. Average metabolic rates of heat production and rates of heat loss for Meas. 1 and Meas. 3 and both sitting and standing positions.

Heat Rate	Meas. 1 (Sitting)	Meas. 1 (Standing)	Meas. 3 (Sitting)	Meas. 3 (Standing)
M ($W/(m^2K)$)	58.8	69.8	58.1	69.8
Q_{res} ($W/(m^2K)$)	5.3	6.0	5.4	6.5
$Q_{cr,s}$ ($W/(m^2K)$)	54.3	64.0	36.7	51.9
$Q_{ev,s}$ ($W/(m^2K)$)	2.8	6.4	4.5	14.0
Q_{cd} ($W/(m^2K)$)	71.7	0.0	29.2	0.0
Q_{tot} ($W/(m^2K)$)	134.2	76.4	75.9	72.4

Based on the computed heat exchange parameters, the average core and skin temperatures are computed for Meas. 1 and Meas. 3 and both sitting and standing positions via Equations (A1) and (A2) (see Figure A3).

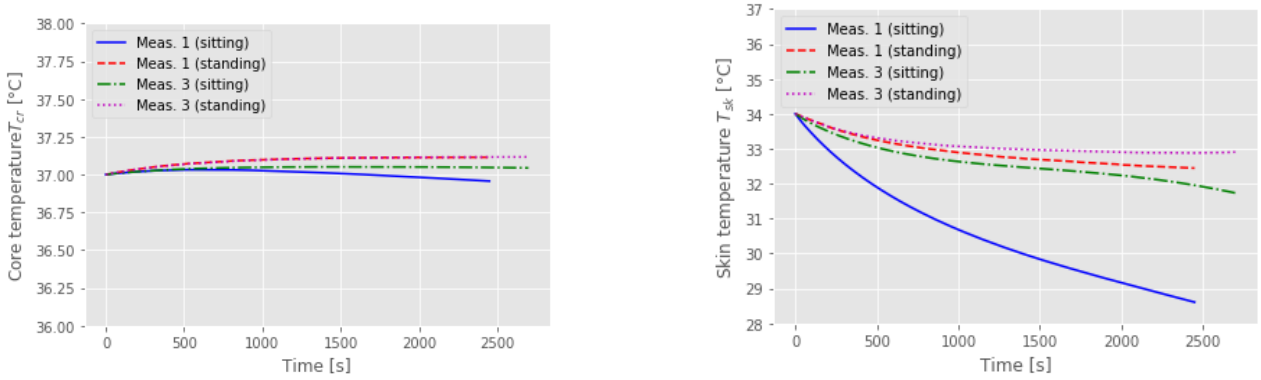

(**a**) Core temperature T_{cr}

(**b**) Skin temperature T_{sk}

Figure A3. Computed average (**a**) core and (**b**) skin temperatures for Meas. 1 and Meas. 3 and both sitting and standing positions.

Notice that the core temperature T_{cr} varies minimally throughout time for all measurements, whereas the skin temperature T_{sk} can change of several degrees depending on the external climatic conditions. This change is particularly significant for sitting positions during Meas. 1. In this case, T_{sk} decreases of up to 5.4 °C from the beginning to the end of the measurement.

References

1. *Climate Watch*; The World Resource Institute: Washington, DC, USA, 2020.
2. Friedlingstein, P.; Jones, M.; O'sullivan, M.; Andrew, R.; Hauck, J.; Peters, G.; Peters, W.; Pongratz, J.; Sitch, S.; DBakker, O.; et al. Global Carbon Budget 2019. *Earth Syst. Sci. Data* **2019**, *11*, 1783–1838. [CrossRef]
3. *Zero and Low Carbon Mobility*; Technical Report; German Partnership for Sustainable Mobility: Eschborn, Germany, 2015.
4. Bmub, D.K.I. (Ed.) *Climate Action Plan 2050*; Federal Ministry for the Environment, Nature Conservation, Building and Nuclear Safety (BMUB): Bonn, Germany, 2016.
5. juris GmbH. *VIS BE §1 MobG BE | Landesnorm Berlin | -Zweck des Gesetzes | Berliner Mobilitätsgesetz vom 5. Juli 2018 | gültig ab: 18.07.2018*; juris GmbH: Berlin, Germany, 2018.
6. Göhlich, D.; Fay, T.A.; Jefferies, D.; Lauth, E.; Kunith, A.; Zhang, X. Design of urban electric bus systems. *Des. Sci.* **2018**, *4*. [CrossRef]

7. VDV-Schrift Nr. 236. *Klimatisierung von Linienbussen der Zulassungsklassen I (Stadtbus) und II (Überlandbus), für konventionell angetriebene Diesel- und Gasbusse als auch für Hybrid-, Brennstoffzellen- und Elektrobusse*; Verband Deutscher Verkehrsunternehmen e.V.: Berlin, Germany, 2009.
8. *ASHRAE Handbook Fundamentals*; ASHRAE, American Society of Heating, Refrigerating and Air–Conditioning Engineers, Inc.: Peachtree Corners, GA, USA, 2017.
9. Gagge, A.P.; Stolwijk, J.; Nishi, Y. An Effective Temperature Scale Based on a Simple Model of Human Physiological Regulatiry Response. *ASHRAE Trans.* **1971**, *70 Pt 1*, 21–36.
10. Gagge, A.P.; Fobelets, A.P.; Berglund, L.G. A Standard Predictive Index of Human Response to the Thermal Environment. *ASHRAE Trans.* **1986**, *92 Pt 2*, 709–731.
11. Fanger, P.O. *Thermal Comfort: Analysis and Applications in Environmental Engineering*; R.E. Krieger Pub. Co.: Malabar, FL, USA, 1982.
12. Kaynakli, O.; Pulat, E.; Kilic, M. Thermal comfort during heating and cooling periods in an automobile. *Heat Mass Transf.* **2005**, *41*, 449–458. [CrossRef]
13. Kaynakli, O.; Kilic, M. An investigation of thermal comfort inside an automobile during the heating period. *Appl. Ergon.* **2005**, *36*, 301–312. [CrossRef] [PubMed]
14. Pala, U.; Oz, H.R. An investigation of thermal comfort inside a bus during heating period within a climatic chamber. *Appl. Erogonomics* **2015**, *48*, 164–176. [CrossRef] [PubMed]
15. Kimmling, M.; Hoffmann, S. Behaglichkeitsmonitoring–flächendeckend und kostengünstig mit der Sensorstation CoMoS. *Bauphysik* **2019**, *41*, 111–119. [CrossRef]
16. Koester, R.A.; Saleh, Y.A.; Roihan, I.; Harinaldi. A simple method for calibration of temperature sensor DS18B20 waterproof in oil bath based on Arduino data acquisition system. *AIP Conf. Proc.* **2019**, *2032*, 020006.
17. Schmidt, C. Entwicklung Eines Modellansatzes zur Bewertung der Thermischen Behaglichkeit unter Inhomogenen Klimabedingungen. Ph.D. Thesis, Technischen Hochschule Aachen, Aachen, Germany, 2016.
18. Du Bois, D.; Du Bois, E.F. A formula to estimate the approximate surface area if height and weight be known. *Arch. Intern. Med.* **1916**, *17*, 863–871. [CrossRef]
19. ISO 7726. *Ergonomics of the Thermal Environment-Instrument for Measuring Physical Quantities*; International Organization for Standardization: Geneva, Switzerland, 1998.
20. Mitchell, D. *Heat Loss from Animals and Man*; Chapter Convective Heat Transfer in Man and Other Animals; Butterworth Publishing: Oxford, UK, 1974.
21. Seppänen, O.; McNall, P.; Munson, D.; Sprague, C. Thermal insulating values for typical indoor clothing ensembles. *ASHRAE Trans.* **1972**, *78*, 120–130.